Efficient computational model of the in-flow capturing of magnetic nanoparticles by a cylindrical magnet for cancer nanomedicine

Barbara Wirthl [1,*] Vitaly Wirthl [2] and Wolfgang A. Wall [1]

[1]*Institute for Computational Mechanics, Technical University of Munich, TUM School of Engineering and Design, Department of Engineering Physics & Computation, Garching bei München, 85748 Garching, Germany*
[2]*Max Planck Institute of Quantum Optics (MPQ), Garching bei München, 85748 Garching, Germany*

Magnetic nanoparticles have emerged as a promising approach to improving cancer treatment. However, many nanoparticle designs fail in clinical trials due to a lack of understanding of how to overcome the *in vivo* transport barriers. To address this shortcoming, we develop a computational model aimed at the study of magnetic nanoparticles *in vitro* and *in vivo*. In this paper, we present an important building block for this overall goal, namely an efficient computational model of the in-flow capture of magnetic nanoparticles by a cylindrical permanent magnet in an idealized test setup. We use a continuum approach based on the Smoluchowski advection-diffusion equation, combined with a simple approach to consider the capture at an impenetrable boundary, and derive an analytical expression for the magnetic force of a cylindrical magnet of finite length on the nanoparticles. This provides a simple and numerically efficient way to study different magnet configurations and their influence on the nanoparticle distribution in three dimensions. Such an *in silico* model can increase insight into the underlying physics, help to design prototypes, and serve as a precursor to more complex systems *in vivo* and *in silico*.

I. INTRODUCTION

Over the past three decades, nanoparticles have emerged as a promising approach to improve the effectiveness of cancer treatment because of their potential for sophisticated functionalization and ability to accumulate in tumours [1]. Magnetic nanoparticles are of particular interest because of their ability to be controlled by an external magnetic field. To capture the drug-loaded magnetic nanoparticles in the target region, the applied magnetic force has to be strong enough to overcome fluid forces due to the blood flow or the interstitial fluid flow and further transport barriers, e.g., the extracellular matrix, the blood vessel wall, which the nanoparticles must cross, and different interfaces. However, this is often hard to achieve because of the inherently weak magnetic forces produced by an applied magnetic field—especially deeper in the body [2]. Because of those (and other) challenges, the design and successful application of magnetic nanoparticle-based cancer therapy is very demanding and almost hopeless purely via trial-and-error approaches in experimental research. Here, computational models can help by predicting the distribution of nanoparticles depending on the applied magnetic field and guide the design of prototypes.

On the way towards a comprehensive computational model of the capture of magnetic nanoparticles, we here start with an idealized test setup, illustrated in Fig. 1: a cylindrical permanent magnet is placed below a channel to capture the magnetic nanoparticles dispersed in the fluid flowing through the

channel. This setup, even though simplified, contains the essential physics of the capture of magnetic nanoparticles: the magnetic force exerted by the magnet combined with the fluid flow, which is known to be a major transport barrier *in vivo* [1]. The bottom wall of the domain is impenetrable, so the captured nanoparticles accumulate at the wall. Such an idealized test setup, including tumour spheroids in the microfluidic channel, is typically used in experimental research, e.g., Refs. [3–5], because it allows insight into the fundamental physics of the capture of magnetic nanoparticles and serves as a precursor to more complex *in vivo* systems. The approaches and results of the current work are essential for exactly modeling the experimental setup where tumour spheroids are placed in the microfluidic channel [6].

To model the transport of magnetic nanoparticles, two approaches are the most common in the literature [7]: the first approach models the nanoparticles as discrete particles, while the second approach assumes that the nanoparticles behave as a continuum ferrofluid. The first approach considers the different forces acting on each particle individually, and Newton's second law then describes the movement of each particle [8–11]. This allows investigating the aggregation of the nanoparticles and the formation of particle clusters, e.g., chains [10,11]. Nevertheless, when the system has a size of millimetres or centimetres, the number of particles in the domain is on the order of 10^9, which limits the applicability of this approach. Moreover, we are not interested in the movement of each particle individually. The second approach builds on the assumption that the nanoparticles have an infinitely strong coupling with the base fluid, and this fluid-particle mixture is described as a whole by the classical fluid

---

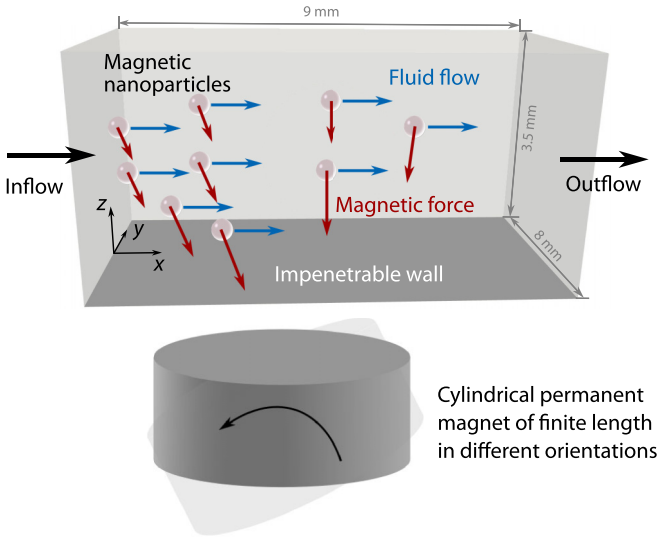*Contact author: barbara.wirthl@tum.de

FIG. 1. Idealized test setup. The magnetic nanoparticles are dispersed in the fluid flowing through the channel. A cylindrical permanent magnet is placed below the channel and exerts a magnetic force on the magnetic nanoparticles to capture them at the bottom wall, which is impenetrable.

equations, e.g., the Navier–Stokes equations [12–15]. Hence, the magnetic force is part of the momentum balance equation. This approach, however, does not allow the nanoparticles to move relative to the fluid [15].

To overcome the limitations of both approaches, we take a different approach here, similar to Ref. [16]: We model the nanoparticles in a continuum sense but consider that the nanoparticles can move relative to the advecting fluid due to diffusion and the exerted magnetic force. We therefore use an advection-diffusion equation to model the concentration of the nanoparticles and include the magnetic force directly in this equation. In this contribution, we address two specific challenges: the boundary condition at an impenetrable boundary and the efficient evaluation of the magnetic force exerted by a cylindrical magnet of finite length.

Concerning the first challenge (the boundary condition at an impenetrable boundary), Ref. [15] states that most contributions in the literature that study the transport of magnetic nanoparticles in a continuum sense do not consider the boundary condition at the impenetrable boundary, which results in nanoparticles leaving the domain through the boundary. This however would be questionable for our long-term goal, as we also want to be able to model complex time-dependent scenarios where we should not lose nanoparticles. Hence, we present a simple approach to model the capture of magnetic nanoparticles at an impenetrable boundary.

Concerning the second challenge (the efficient evaluation of the magnetic force), we derive an analytical expression for the magnetic force on magnetic nanoparticles exerted by a cylindrical magnet of finite length. This presents a huge advantage of our approach, as it allows us to evaluate the magnetic force on the nanoparticles with minimal computational effort compared to numerically solving Maxwell's equations. At the same time, we can study different magnet orientations in three dimensions—in contrast to two-dimensional models,

commonly used in the literature [2,16–20], which have the severe limitation that they assume the magnet to be infinitely long and oriented perpendicular to the two-dimensional domain.

In the following, we first introduce the equations for the advection-diffusion problem, including an impenetrable boundary, in Sec. II A. We then present the analytical expression for the magnetic force on the nanoparticles in Sec. II B. Section III presents and discusses numerical examples for both and Sec. IV draws a conclusion.

II. METHODS

A. Transport of nanoparticles: Smoluchowski advection-diffusion equation

We assume that the magnetic nanoparticles are dispersed in the fluid in a stable colloidal suspension, so the particle concentration ϕ^{NP} is small ($\phi^{NP} \ll 1$). We therefore assume that nanoparticles do not interact with each other, i.e., we neglect the interparticle forces for now, and we assume that the nanoparticles do not influence the fluid flow. Here, we interpret ϕ^{NP} as the (dimensionless) mass fraction of the nanoparticles in the fluid. In general, ϕ can be any intensive quantity, e.g., mass concentration, volume concentration, or molar concentration.

The concentration of the nanoparticles ϕ^{NP} is governed by the mass balance equation

$$\frac{\partial \phi^{NP}}{\partial t} + \nabla \cdot \boldsymbol{q}_{\text{tot}} = 0, \tag{1}$$

where $\boldsymbol{q}_{\text{tot}}$ denotes the total flux. Here, we assume that neither sources nor sinks are present. The total flux is the sum of three contributions,

$$\boldsymbol{q}_{\text{tot}} = \boldsymbol{q}_{\text{diff}} + \boldsymbol{q}_{\text{adv}} + \boldsymbol{q}_{\text{mag}}, \tag{2}$$

arising from diffusion, advection, and the magnetic force, respectively.

First, the diffusive flux $\boldsymbol{q}_{\text{diff}}$ arises from a local concentration gradient $\nabla \phi^{NP}$ and is described by Fick's first law,

$$\boldsymbol{q}_{\text{diff}} = -D \nabla \phi^{NP}, \tag{3}$$

with the diffusion coefficient D. Second, the advective flux $\boldsymbol{q}_{\text{adv}}$ arises from the velocity $\boldsymbol{v}_{\text{adv}}$ of the fluid advecting the nanoparticles and is given by

$$\boldsymbol{q}_{\text{adv}} = \boldsymbol{v}_{\text{adv}} \phi^{NP}.$$

The fluid velocity $\boldsymbol{v}_{\text{adv}}$ might be given by solving the underlying flow problem, e.g., the Navier–Stokes equations or Darcy flow in a porous medium. For the sake of simplicity in this paper, we here directly prescribe the velocity of the fluid.

When the nanoparticles are not only subjected to fluid flow but additionally to a magnetic force, we include an additional magnetophoretic flux $\boldsymbol{q}_{\text{mag}}$ depending on the magnetic force $\boldsymbol{F}_{\text{mag}}$. Typically, the resulting magnetophoretic velocity $\boldsymbol{v}_{\text{mag}}$ is assumed to be directly proportional to the applied force, e.g., see Refs. [16,21], resulting in a magnetophoretic flux of

$$\boldsymbol{q}_{\text{mag}} = \boldsymbol{v}_{\text{mag}} \phi^{NP} \quad \text{with} \quad \boldsymbol{v}_{\text{mag}} = \zeta^{-1} \boldsymbol{F}_{\text{mag}}, \tag{4}$$

where $\zeta = 6\pi \mu^{\ell} R^{NP}$ is the mobility of a particle of radius R^{NP} in a fluid with dynamic viscosity μ^{ℓ}, based on

Stokes' law. Note that μ^ℓ denotes the dynamic viscosity of the fluid by the superscript ℓ (*liquid*) to distinguish it from the magnetic vacuum permeability μ_0 which we will introduce in Sec. II B. Altogether, this results in the Smoluchowski advection-diffusion equation [22]

$$\frac{\partial \phi^{\mathrm{NP}}}{\partial t} - \nabla \cdot (D \nabla \phi^{\mathrm{NP}}) + \nabla \cdot (\mathbf{v}_{\mathrm{adv}} \phi^{\mathrm{NP}})$$
$$+ \nabla \cdot (\zeta^{-1} \mathbf{F}_{\mathrm{mag}} \phi^{\mathrm{NP}}) = 0. \tag{5}$$

Equation (4) assumes that the velocity is always directly proportional to the applied force. Now consider an example of a channel with an impenetrable wall and a force perpendicular to the wall, as sketched in Fig. 1: The force results in a velocity perpendicular to the wall, which in turn results in the nanoparticles leaving the domain through the impenetrable wall—which is obviously not physical.

We therefore introduce the mobility tensor $\boldsymbol{\mathcal{M}}$, which relates the magnetophoretic velocity to the magnetic forces, i.e.,

$$\mathbf{v}_{\mathrm{mag}} = \boldsymbol{\mathcal{M}} \mathbf{F}_{\mathrm{mag}}, \tag{6}$$

or more explicitly,

$$\begin{bmatrix} v_x \\ v_y \\ v_z \end{bmatrix} = \begin{bmatrix} \mathcal{M}_{xx} & \mathcal{M}_{xy} & \mathcal{M}_{xz} \\ \mathcal{M}_{yx} & \mathcal{M}_{yy} & \mathcal{M}_{yz} \\ \mathcal{M}_{zx} & \mathcal{M}_{zy} & \mathcal{M}_{zz} \end{bmatrix} \begin{bmatrix} F_x \\ F_y \\ F_z \end{bmatrix}, \tag{7}$$

similar to Refs. [23,24] who used the same concept in a different context. The mobility is a tensor field $\boldsymbol{\mathcal{M}}(\mathbf{x})$ that depends on the position $\mathbf{x}$. Now, a force in a specific direction does not necessarily result in a velocity in that direction, but only if the particle can move in this direction, i.e., if the mobility is nonzero. At an impenetrable wall, the nanoparticles cannot move in the direction perpendicular to the wall, i.e., into the wall, and thus the mobility is zero in this direction, resulting also in zero velocity. All off-diagonal entries of the mobility tensor $\boldsymbol{\mathcal{M}}$ are also zero in our case: a force in one direction only causes a velocity in the same direction and no "shear" velocity. Inside the domain, $\mathcal{M}_{xx} = \mathcal{M}_{yy} = \mathcal{M}_{zz} = \zeta^{-1}$, which reduces back to Eq. (4). At the impenetrable wall (at $z = 0$), the diagonal entries tangential to the wall still equal the scalar mobility, i.e., $\mathcal{M}_{xx} = \mathcal{M}_{yy} = \zeta^{-1}$. However, the entry perpendicular to the wall is zero $\mathcal{M}_{zz} = 0$, as already mentioned above. The mobility tensor at the impenetrable wall is thus given by

$$\boldsymbol{\mathcal{M}}_{\mathrm{wall}} = \begin{bmatrix} \zeta^{-1} & 0 & 0 \\ 0 & \zeta^{-1} & 0 \\ 0 & 0 & 0 \end{bmatrix}. \tag{8}$$

The key point here is that we employ the mobility as a tensor field—as opposed to a scalar.

The final form of the Smoluchowski advection-diffusion equation is then given by

$$\frac{\partial \phi^{\mathrm{NP}}}{\partial t} - \nabla \cdot (D \nabla \phi^{\mathrm{NP}}) + \nabla \cdot (\mathbf{v}_{\mathrm{adv}} \phi^{\mathrm{NP}})$$
$$+ \nabla \cdot (\boldsymbol{\mathcal{M}} \mathbf{F}_{\mathrm{mag}} \phi^{\mathrm{NP}}) = 0. \tag{9}$$

We solve this partial differential equation in time and space for the concentration of the nanoparticles ϕ^{NP}. For time

discretization, we use the backward Euler method with a time step size Δt and initial conditions specified at $t = 0$. For spatial discretization, we use the finite element method (FEM). We first employ the standard Galerkin procedure to obtain the weak form of Eq. (9), i.e., we multiply the strong form of the equation by a test function and integrate over the domain. We apply Gauss' theorem to terms containing a second spatial derivative, i.e., the diffusion term in our case, to decrease the differentiability requirements of the solution function space. We then discretize in space using linear shape functions, i.e., quadrilateral elements in two dimensions and hexahedral elements in three dimensions. Finally, the resulting system of equations is solved using one Newton–Raphson loop per time step to obtain the solution at the nodes of the mesh. More details on the concepts of FEM can be found in textbooks, e.g., Refs. [25,26]. We use our in-house parallel multiphysics research code 4C [27] as a computational framework.

Remark (Stabilization). In our case, Eq. (9) is dominated by the two convective terms, which causes numerical instabilities when using the standard Galerkin procedure. To stabilize the equation, we use the streamline upwind Petrov–Galerkin (SUPG) method [28], which introduces numerical diffusion along streamlines in a consistent manner [29]. We choose the stabilization parameter τ based on Ref. [30].

B. Magnetic force on the nanoparticles

Due to the permanent magnet, the magnetic nanoparticles are subjected to a static nonhomogenous external magnetic field $\mathbf{H}$ leading to a force $\mathbf{F}_{\mathrm{mag}}$. This force however does not only depend on the magnetic field but also the magnetic response of the particles.

Due to the small size of the particles, we assume that they can be modeled as an equivalent point dipole located at the center of the particle (*effective dipole moment approach* [7,16,31]). Also, due to the small size, the nanoparticles are superparamagnetic: They are magnetized with a large magnetic susceptibility χ^{NP} when an external magnetic field is applied but do not retain their magnetization after the external magnetic field is removed. Hence, when a superparamagnetic nanoparticle is placed in an external magnetic field, it magnetises, resulting in a magnetic moment $\mathbf{m}^{\mathrm{NP}}$. The force on the magnetic dipole induced in the nanoparticle is then given by

$$\mathbf{F}_{\mathrm{mag}} = \mu_0 (\mathbf{m}^{\mathrm{NP}} \cdot \nabla) \mathbf{H}, \tag{10}$$

with the magnetic vacuum permeability μ_0. Note that we assume that the fluid (in our case, water) and air are nonmagnetic, and thus assume that their permeability is equal to the vacuum magnetic permeability, given by $\mu_0 = 1.25663706212(19) \times 10^{-6}\,\mathrm{N/A^2}$ [32]. The exact values for water and air differ from the value for vacuum at the fifth and seventh decimal places, respectively. Using the magnetization $\mathbf{M}^{\mathrm{NP}}$ as the magnetic moment per volume, i.e., $\mathbf{M}^{\mathrm{NP}} = \mathbf{m}^{\mathrm{NP}}/V^{\mathrm{NP}}$ with V^{NP} being the volume of the nanoparticle, the force can be written as

$$\mathbf{F}_{\mathrm{mag}} = \mu_0 V^{\mathrm{NP}} (\mathbf{M}^{\mathrm{NP}} \cdot \nabla) \mathbf{H}. \tag{11}$$

Thus, the force depends on the magnetization of the nanoparticle and the derivatives of the applied magnetic field.
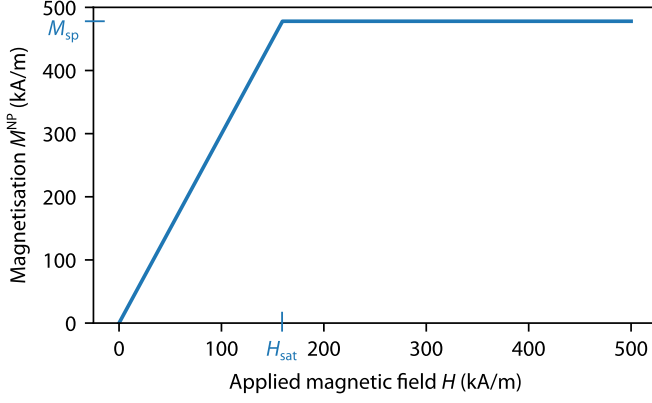
FIG. 2. Magnetization curve for a superparamagnetic nanoparticle with linear magnetization and saturation above an applied magnetic field of H_{sat}, assuming a saturation magnetization of $M_{\text{sp}} = 478\,\text{kA}\,\text{m}^{-1}$ [16] and magnetic susceptibility of $\chi^{\text{NP}} \gg 1$ [16,36,37].

The magnetized nanoparticles also produce a magnetic field, affecting the nearby nanoparticles. For now, we assume that the magnetic force that the nanoparticles exert on each other is negligible compared to the magnetic force exerted by the external magnetic field—which is a valid assumption for low concentrations of nanoparticles and hence large distances between the nanoparticles [15,16,33–35]. We will investigate and discuss the validity of this assumption in Sec. III C.

1. Magnetization model

To relate the magnetization of the nanoparticle to the applied magnetic field, we use a linear magnetization model with saturation, given by

$$M^{\text{NP}} = f(|H|)H, \tag{12}$$

with

$$f(|H|) = \begin{cases} \frac{3\chi^{\text{NP}}}{3+\chi^{\text{NP}}} & \text{if } |H| < H_{\text{sat}}, \\ \frac{M_{\text{sp}}}{|H|} & \text{if } |H| \geqslant H_{\text{sat}}, \end{cases} \tag{13}$$

with M_{sp} being the saturation magnetization and H_{sat} the field strength for which the particle reaches saturation, as presented by Refs. [7,16,21]. An example of such a magnetization curve is shown in Fig. 2. If the particle is below saturation, then its magnetization is proportional to the applied magnetic field

$$M^{\text{NP}} = \frac{3\chi^{\text{NP}}}{3+\chi^{\text{NP}}}H, \tag{14}$$

and the particle reaches saturation for

$$H_{\text{sat}} = \frac{\chi^{\text{NP}}+3}{3\chi^{\text{NP}}}M_{\text{sp}}, \tag{15}$$

which can be derived based on the effective dipole moment approach [16,31]. Above saturation, the magnetization is equal to the saturation magnetization M_{sp},

$$M^{\text{NP}} = M_{\text{sp}}\frac{H}{|H|}. \tag{16}$$

The magnetization is always aligned with the applied magnetic field.

Finally, as discussed above, the particles are superparamagnetic: Their magnetic susceptibility is much higher than the magnetic susceptibility of paramagnetic materials, i.e., $\chi^{\text{NP}} \gg 1$ [16,36,37]. Equation (13) can then be simplified to

$$f(|H|) = \begin{cases} 3 & \text{if } |H| < \frac{1}{3}M_{\text{sp}}, \\ \frac{M_{\text{sp}}}{|H|} & \text{if } |H| \geqslant \frac{1}{3}M_{\text{sp}}. \end{cases} \tag{17}$$

In sum, the magnetic force on the nanoparticles is given by

$$\boldsymbol{F}_{\text{mag}} = \mu_0 V^{\text{NP}} f(|H|)(\boldsymbol{H} \cdot \boldsymbol{\nabla})\boldsymbol{H}, \tag{18}$$

which shows that the magnetic force depends both on the strength of the magnetic field and its derivatives.

2. Analytical expression for the magnetic field

Usually, the magnetic field $\boldsymbol{H}$ is obtained by solving Maxwell's equations numerically. Analytic expressions are only well-known for some classic textbook cases: the magnetic field of point multipoles and infinitely long wires carrying a current [38]. However, for a finite-length cylindrical magnet, which we have here, Derby and Olbert [39] and Caciagli et al. [40] presented analytic expressions based on the elliptic integrals. These analytic expressions are beneficial because the magnetic quantities can be evaluated at all coordinates with minimal computational effort compared to numerically solving Maxwell's equations, e.g., using the FEM. In the following, we summarize the analytic expression for the magnetic field, as presented by Refs. [39,40], and then extend this by deriving the analytic expressions for the magnetic force.

The cylindrical magnet is magnetized in the longitudinal direction. The field components of the magnetic field $\boldsymbol{H}$ in cylindrical coordinates (ρ, ϕ, z) are given by

$$H_\rho(\rho, z) = \frac{M_s R_{\text{mag}}}{\pi}[\alpha_+ P_1(k_+) - \alpha_- P_1(k_-)] \tag{19a}$$

and

$$H_z(\rho, z) = \frac{M_s R_{\text{mag}}}{\pi(\rho + R_{\text{mag}})}[\beta_+ P_2(k_+) - \beta_- P_2(k_-)] \tag{19b}$$

and $H_\phi = 0$ due to the radial symmetry of the system [39,40]. Here, M_s denotes the magnetization of the cylindrical magnet and R_{mag} its radius. The origin of the cylindrical coordinate system is located at the center of the magnet. Equations (19) are mathematically well-behaved except on the edge of the magnet at $\rho = \pm R_{\text{mag}}$ and $z = \pm\frac{L_{\text{mag}}}{2}$ [39]. The two auxiliary functions P_1 and P_2 are defined as

$$P_1(k) = \mathcal{K}(1-k^2) - \frac{2}{1-k^2}[\mathcal{K}(1-k^2) - \mathcal{E}(1-k^2)], \tag{20a}$$

$$P_2(k) = -\frac{\gamma}{1-\gamma^2}[\Pi(1-\gamma^2, 1-k^2) - \mathcal{K}(1-k^2)]$$
$$- \frac{1}{1-\gamma^2}[\gamma^2\Pi(1-\gamma^2, 1-k^2) - \mathcal{K}(1-k^2)]. \tag{20b}$$

with the following auxiliary variables

$$\rho_{\pm} = R_{\text{mag}} \pm \rho, \quad \zeta_{\pm} = \frac{L_{\text{mag}}}{2} \pm z, \quad \alpha_{\pm} = \frac{1}{\sqrt{\zeta_{\pm}^2 + \rho_{+}^2}},$$

$$\beta_{\pm} = \zeta_{\pm}\alpha_{\pm}, \quad \gamma = -\frac{\rho_{-}}{\rho_{+}}, \quad k_{\pm} = \sqrt{\frac{\zeta_{\pm}^2 + \rho_{-}^2}{\zeta_{\pm}^2 + \rho_{+}^2}},$$

and L_{mag} being the length of the cylindrical magnet.

Equations (20) are based on the complete elliptic integrals of the first, second, and third kind, which in Legendre's notation are written as

$$\mathcal{K}(m) = \int_0^{\pi/2} \frac{d\theta}{\sqrt{1 - m\sin^2\theta}}, \tag{21a}$$

$$\mathcal{E}(m) = \int_0^{\pi/2} \sqrt{1 - m\sin^2\theta}\, d\theta, \tag{21b}$$

$$\Pi(n, m) = \int_0^{\pi/2} \frac{d\theta}{(1 - n\sin^2\theta)\sqrt{1 - m\sin^2\theta}}. \tag{21c}$$

All three kinds of elliptic integrals can be efficiently evaluated using Carlson's functions R_F, F_D, and R_J [41,42] as

$$\mathcal{K}(m) = R_F(0, 1 - m, 1), \tag{22a}$$

$$\mathcal{E}(m) = R_F(0, 1 - m, 1) - \frac{m}{3}R_D(0, 1 - m, 1), \tag{22b}$$

$$\Pi(n, m) = R_F(0, 1 - m, 1) + \frac{n}{3}R_J(0, 1 - m, 1 - n). \tag{22c}$$

Numerical Recipes [43] provides algorithms and source code for evaluating Carlson's functions, which are also implemented in Mathematica [44] and SciPy [45].

Remark (Parameter and sign conventions in the elliptic integrals). Note that Numerical Recipes [43, p. 315] uses a different sign convention for the variable n in the third elliptic integral, such that

$$\Pi(n, m) = \int_0^{\pi/2} \frac{d\theta}{(1 + n\sin^2\theta)\sqrt{1 - m\sin^2\theta}}$$

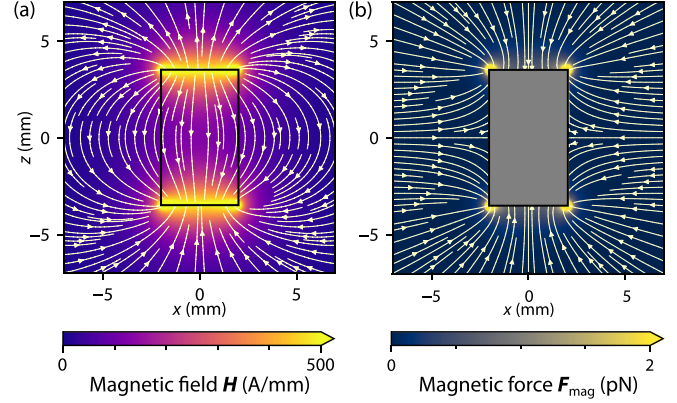$$= R_F(0, 1 - m, 1) - \frac{n}{3}R_J(0, 1 - m, 1 + n).$$

FIG. 3. Magnetic field $\boldsymbol{H}$ (a) and magnetic force $\boldsymbol{F}_{\text{mag}}$ (b) on the nanoparticles of a cylindrical magnet with radius $R_{\text{mag}} = 2$ mm and length $L_{\text{mag}} = 7$ mm.

Additionally, Ref. [40] uses the convention with parameter k, where $m = \tilde{k}^2 = \sqrt{1 - k^2}$ in their Eq. (6) in Ref. [40]. Mathematica [44] and SciPy [45] however use the parameter m, as presented here in Eqs. (21).

Figure 3(a) shows an example of the magnetic field $\boldsymbol{H}$ of a cylindrical magnet with radius $R_{\text{mag}} = 2$ mm, length $L_{\text{mag}} = 7$ mm and magnetization $M_s = 1 \times 10^6$ Am^{-1}. Inside the magnet, the magnetic field is given by $\boldsymbol{H} = \frac{\boldsymbol{B}}{\mu_0} - \boldsymbol{M}_s$, with the magnetic flux density $\boldsymbol{B}$. For a longitudinally magnetized magnet, the magnetization vector is $\boldsymbol{M}_s = M_s\boldsymbol{e}_z$, with $\boldsymbol{e}_z$ being the unit vector in z direction. The magnetization vector is constant inside and zero outside the magnet. The result for the magnetic field $\boldsymbol{H}$ in Fig. 3(a) is qualitatively well known: the magnetic field lines start at one pole and end at the other, forming fanned-out circular segments around the magnet.

3. Analytical expression for the magnetic force

As discussed above, the magnetic force $\boldsymbol{F}_{\text{mag}}$ depends on the magnetic field and its derivatives. Since the first derivatives of the elliptic integrals are known analytically, we can derive an analytical expression for the magnetic force $\boldsymbol{F}_{\text{mag}}$. Evaluating Eq. (18) for the analytical expression for the magnetic field, given by Eqs. (19), results in the force components given by

$$F_\rho(\rho, z) = \frac{\mu_0 V^{\text{NP}} f(|\boldsymbol{H}|)M_s^2}{4\pi^2 \rho_+ \rho^3 a_1 a_2 a_3 a_4}\left[\left(\frac{a_4 c_1 \zeta_+ \mathcal{E}(\psi_+)}{\alpha_-} + \frac{a_3 c_2 \zeta_- \mathcal{E}(\psi_-)}{\alpha_+} - \frac{a_3 a_4 \zeta_+ \mathcal{K}(\psi_+)}{\alpha_-} - \frac{a_3 a_4 \zeta_- \mathcal{K}(\psi_-)}{\alpha_+}\right)\rho^2 Q_2\right.$$

$$\left. + \left(\frac{a_4(b_1^2 + b_3\rho^2)\mathcal{E}(\psi_+)}{\alpha_-} - \frac{a_3(b_2^2 + b_4\rho^2)\mathcal{E}(\psi_-)}{\alpha_+} + \frac{a_3 a_4 b_2 \mathcal{K}(\psi_-)}{\alpha_+} - \frac{a_3 a_4 b_1 \mathcal{K}(\psi_+)}{\alpha_-}\right)\rho_+ Q_1\right] \tag{23a}$$

and

$$F_z(\rho, z) = \frac{\mu_0 V^{\text{NP}} f(|\boldsymbol{H}|)M_s^2}{4\pi^2 a_1 a_2 a_3 a_4}\left[\left(\frac{a_3 a_4 \zeta_+ \mathcal{K}(\psi_+)}{\alpha_-} + \frac{a_3 a_4 \zeta_- \mathcal{K}(\psi_-)}{\alpha_+} - \frac{a_4 c_1 \zeta_+ \mathcal{E}(\psi_+)}{\alpha_-} - \frac{a_3 c_2 \zeta_- \mathcal{E}(\psi_-)}{\alpha_+}\right)\frac{Q_1}{\rho^2}\right.$$

$$\left. + \left(\frac{a_3 c_4 \mathcal{E}(\psi_-)}{\alpha_+} - \frac{a_4 c_3 \mathcal{E}(\psi_+)}{\alpha_-} + \frac{a_3 a_4 \mathcal{K}(\psi_+)}{\alpha_-} - \frac{a_3 a_4 \mathcal{K}(\psi_-)}{\alpha_+}\right)\frac{Q_2}{\rho_+}\right], \tag{23b}$$

with two auxiliary functions Q_1 and Q_2 based on the elliptic integrals

$$Q_1(\alpha_+, \alpha_-, \psi_+, \psi_-, a_1, a_2, c_1, c_2)$$
$$= \frac{a_2 \mathcal{E}(\psi_-)}{\alpha_+} - \frac{a_1 \mathcal{E}(\psi_+)}{\alpha_-} + \frac{c_1 \mathcal{K}(\psi_+)}{\alpha_-} - \frac{c_2 \mathcal{K}(\psi_-)}{\alpha_+},$$

$$Q_2(\alpha_+, \alpha_-, \psi_+, \psi_-, \rho_+, \rho_-, \zeta_+, \zeta_-, \beta)$$
$$= \frac{\rho_+ \zeta_+ \mathcal{K}(\psi_+)}{\alpha_-} + \frac{\rho_+ \zeta_- \mathcal{K}(\psi_-)}{\alpha_+} + \frac{\rho_- \zeta_+ \Pi(\beta, \psi_+)}{\alpha_-}$$
$$+ \frac{\rho_- \zeta_- \Pi(\beta, \psi_-)}{\alpha_+}.$$

and the following auxiliary variables:

$$\rho_\pm = R_{\text{mag}} \pm \rho, \quad \zeta_\pm = \frac{L_{\text{mag}}}{2} \pm z, \quad \beta = \frac{4\rho R_{\text{mag}}}{\rho_+^2},$$

$$a_1 = \rho_+^2 + \zeta_+^2, \quad a_2 = \rho_+^2 + \zeta_-^2, \quad a_3 = \rho_-^2 + \zeta_+^2,$$

$$a_4 = \rho_-^2 + \zeta_-^2, \quad \alpha_+ = \frac{1}{\sqrt{a_1}}, \quad \alpha_- = \frac{1}{\sqrt{a_2}},$$

$$\psi_+ = \frac{4\rho R_{\text{mag}}}{a_1}, \quad \psi_- = \frac{4\rho R_{\text{mag}}}{a_2}, \quad b_1 = \zeta_+^2 + R_{\text{mag}}^2,$$

$$b_2 = \zeta_-^2 + R_{\text{mag}}^2, \quad b_3 = \zeta_+^2 - R_{\text{mag}}^2, \quad b_4 = \zeta_-^2 - R_{\text{mag}}^2,$$

$$c_1 = b_1 + \rho^2, \quad c_2 = b_2 + \rho^2, \quad c_3 = b_3 + \rho^2,$$

$$c_4 = b_4 + \rho^2.$$

Note that Eqs. (23) are undefined at $\rho = 0$ and $\rho = \pm R_{\text{mag}}$. Outside the magnet, these singularities are removable and $\boldsymbol{F}_{\text{mag}}$ is extendable.

The coordinate transformations from cylindrical coordinates to cartesian coordinates are given by

$$F_x(x, y, z) = F_\rho(\rho, z) \cos(\varphi), \tag{24a}$$

$$F_y(x, y, z) = F_\rho(\rho, z) \sin(\varphi), \tag{24b}$$

$$F_z(x, y, z) = F_z(\rho, z), \tag{24c}$$

with $\rho = \sqrt{x^2 + y^2}$ and $\varphi = \arctan(x/y)$. Note that most programming languages provide a function `arctan2(y,x)`, which is defined for all $x, y \in \mathbb{R}$ and returns the correct angle φ with respect to the quadrant of the point (x, y).

Figure 3(b) shows the magnetic force $\boldsymbol{F}_{\text{mag}}$ for a cylindrical magnet with radius $R_{\text{mag}} = 2 \, \text{mm}$ and length $L_{\text{mag}} = 7 \, \text{mm}$. Calculating the magnetic force is only meaningful outside the magnet. The magnetic force is on the order of pN, similar to the order of magnitude estimated in Ref. [11] for a similar configuration. We also provide a Python implementation of the analytical expressions for the magnetic field and force [46].

III. NUMERICAL EXAMPLES AND DISCUSSION

In the following, we present and discuss numerical examples to demonstrate the capabilities of the proposed model. In Sec. III A, we start with a two-dimensional example where we investigate the influence of the mobility tensor field on the nanoparticle capture at the impenetrable wall. Next, in Sec. III B, we investigate the nanoparticle distribution in

three dimensions for different positions and orientations of a finite-length cylindrical magnet, leveraging the analytic expression for the magnetic force, which we derived. Finally, in Sec. III C, using the analytical expressions for the magnetic field and force, we examine the validity of the assumption that the interparticle forces are negligible compared to the magnetic force exerted by the external magnetic field.

A. Influence of the mobility tensor field

We first present a two-dimensional example where we investigate the influence of the mobility tensor field $\boldsymbol{\mathcal{M}}(\boldsymbol{x})$ on the distribution of the magnetic particles.

The computational setup is depicted in Fig. 4(a). We study a two-dimensional slice in the XZ plane with a size of $9 \, \text{mm} \times 3.5 \, \text{mm}$, which is discretized with 180×70 linear rectangular elements. The time step size is $\Delta t = 1 \, \text{s}$ and the total simulation time is $150 \, \text{s}$. For simplicity, we consider a constant advective flow velocity $v_{\text{adv}} = 0.1 \, \text{mms}^{-1}$ along the x axis and a constant magnetic force $F_{\text{mag}} = 0.2 \, \text{pN}$ along the z axis, which is a reasonable order of magnitude for the considered cylindrical magnets [see Fig. 3(b)]. For a waterlike fluid with a viscosity of $\mu^\ell = 1 \times 10^{-3} \, \text{Pas}$ and nanoparticles with a radius of $R^{\text{NP}} = 100 \, \text{nm}$, this corresponds to a magnetophoretic velocity of $v_{\text{mag}} \approx 0.1 \, \text{mms}^{-1}$. We assume a diffusion coefficient of $D = 3 \times 10^{-3} \, \text{mm}^2 \, \text{s}^{-1}$. On the in-flow boundary at $x = 0$, we prescribe the concentration of nanoparticles as a Dirichlet boundary condition given by a bell-shaped function with a maximum value of $\phi^{\text{NP}} = 1.0 \times 10^{-6}$. At the initial time $t = 0 \, \text{s}$, the concentration of nanoparticles is zero in the domain apart from the in-flow boundary where it is prescribed by the same bell-shaped function used for the Dirichlet boundary condition.

The wall at the bottom of the domain is impenetrable, and we prescribe a Dirichlet boundary condition for the concentration of nanoparticles given by $\phi^{\text{NP}}_{\text{DBC}} = 0$. Additionally, the z component of the mobility tensor field is zero at the bottom wall, i.e., $\mathcal{M}_{zz} = 0$. We compare the results for the nanoparticle distribution given different functions for $\mathcal{M}_{zz}(z)$, as given in Fig. 4(b). On the one hand, we consider the Heaviside function $\mathcal{M}_{zz}(z) = \mathcal{H}(z - \delta)$, with δ being the boundary layer thickness: this means that the mobility of the nanoparticles is zero in the boundary layer. We choose δ so that the boundary layer is two or three elements wide (given an element size of 0.05). On the other hand, we consider different smooth functions for $\mathcal{M}_{zz}(z)$, which have the value one inside the domain and have different slopes towards the boundary.

Figure 4(c) presents the results given the different functions for $\mathcal{M}_{zz}(z)$. In all cases, the nanoparticles accumulate at the impenetrable wall at the bottom of the domain, which was the primary motivation for introducing the mobility tensor field. All functions lead to a similar distribution of the nanoparticles, with the thickness of the layer of captured nanoparticles depending on the function $\mathcal{M}_{zz}(z)$. However, it shall be noted that the smooth functions are—as to be expected—numerically better behaved than the Heaviside function, which can cause convergence issues.

Defining a tensor field $\boldsymbol{\mathcal{M}}(\boldsymbol{x})$ is a simple way to model the accumulation of nanoparticles at an impenetrable wall. It is worth noting that most similar studies in the literature,
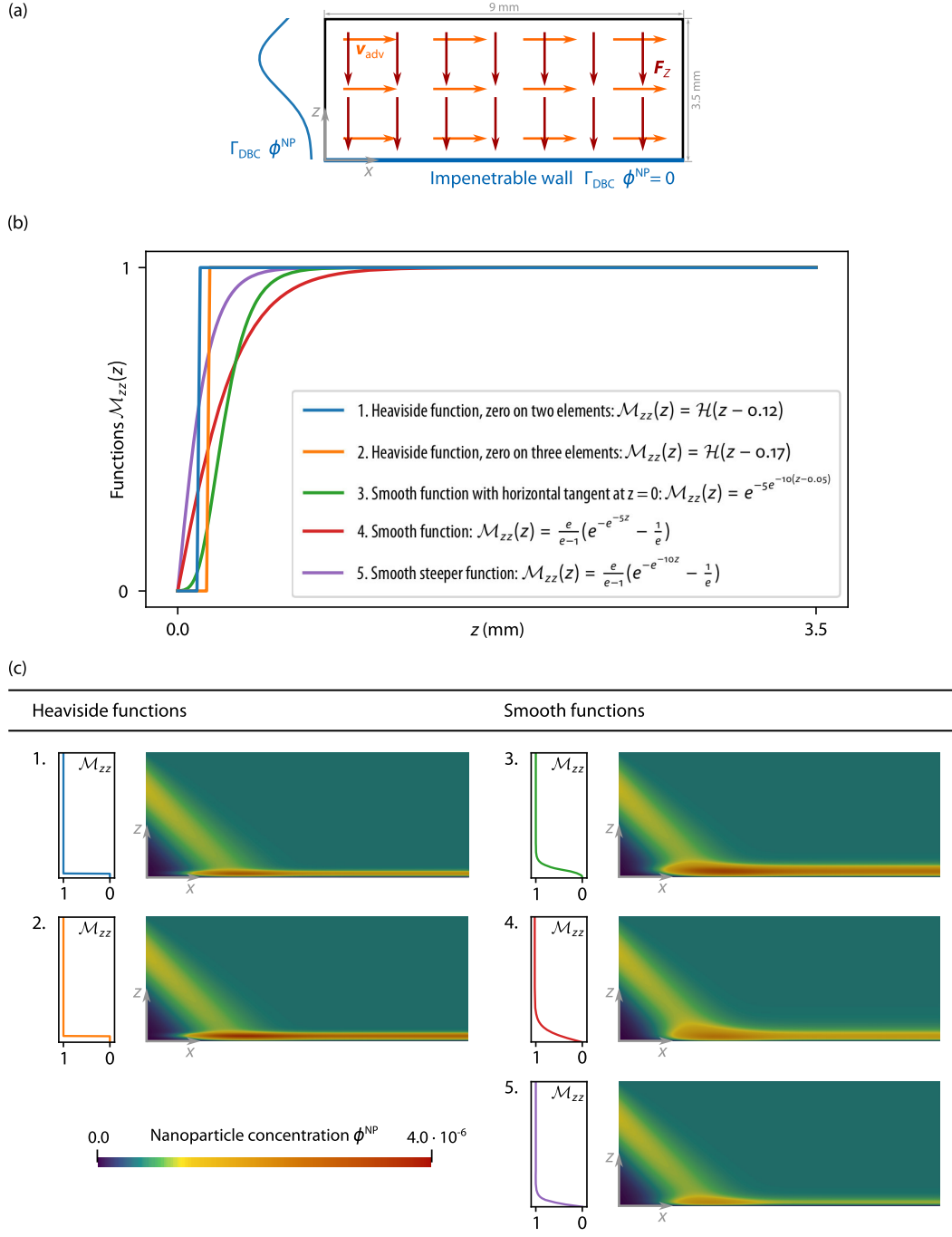
FIG. 4. Investigation of the influence of the mobility tensor field on the nanoparticle distribution (a) Computational setup. (b) Functions for the z-component $\mathcal{M}_{zz}(z)$ of the mobility tensor field. (c) Results for the nanoparticle distributions at $t = 150\,\mathrm{s}$. The colorbar applies to all plots.

e.g., Refs. [16,17,47], do not clarify and also seem to not use appropriate boundary conditions for the nanoparticles at the wall. This allows for studying the trajectories of the nanoparticles in the bulk of the fluid, but it is impossible to investigate the capture of the nanoparticles at a wall. Only Khashan *et al.* [15] presented and discussed an approach for an impermeability condition at the wall: They set the combined advective-diffusive flux to zero,

$$\phi^{\mathrm{NP}}(\boldsymbol{v}_{\mathrm{adv}} + \boldsymbol{v}_{\mathrm{mag}}) \cdot \boldsymbol{n} - D\nabla\phi^{\mathrm{NP}} \cdot \boldsymbol{n} = 0. \qquad (25)$$

We can drop the advective velocity because any physically plausible velocity field cannot have a component perpendicular to an impermeable wall, either by directly imposing a physically plausible velocity field (as we do here) or by prescribing a no-slip boundary condition and solving the fluid equations. Khashan *et al.* [15] subsequently set the normal component of the magnetophoretic velocity at the wall also to zero. Equation (25) then reduces to the classical Neumann boundary condition $D\nabla\phi^{\mathrm{NP}} \cdot \boldsymbol{n} = 0$, which we also impose. In sum, their boundary condition is hence equivalent to our

TABLE I. Parameters for the magnetic nanoparticles, the magnet, and the fluid.

Symbol	Parameter	Value	Units	Ref.
Magnetic nanoparticles				
R^{NP}	Radius of the nanoparticles	100	nm	[16]
D	Diffusion coefficient	3×10^{-3}	$mm^2 s^{-1}$	Assumed
M_{sp}	Saturation magnetization	478	kAm^{-1}	[16]
Magnet				
R_{mag}	Radius of the magnet	2.5	mm	Assumed
L_{mag}	Length of the magnet	5.0	mm	Assumed
M_s	Magnetization of the magnet	1×10^6	Am^{-1}	[16]
Fluid (water)				
μ^{ℓ}	Dynamic viscosity	1×10^{-3}	Pas	Known

approach based on setting the normal component of the mobility tensor to zero, i.e., $\mathcal{M}_{zz} = 0$. Nevertheless, Khashan *et al.* [15] also stated that their employed boundary condition poses a numerical challenge due to the steep concentration gradient at the wall. They solve this problem by prior grid refinement adaptive to the magnetic field gradient. We circumvent it by setting the mobility to zero on several elements or by using a smooth function.

B. Nanoparticle capture with a cylindrical magnet of finite length

We now investigate a three-dimensional example with a cylindrical magnet positioned below the fluid domain. The analytical solution for the magnetic force enables us to efficiently compare different orientations of the magnet.

The computational setup is the one sketched in Fig. 1. It has a size of 9 mm × 4 mm × 3.5 mm, which is discretized with $180 \times 160 \times 70$ linear hexahedral elements. The time step size is again $\Delta t = 1$ s and the total simulated time 150 s. For simplicity, we also again assume a constant advective flow velocity of $v_{adv} = 0.1$ mms^{-1}. The parameters for the magnetic nanoparticles, the magnet and the fluid are given in Table I. The nanoparticle concentration on the in-flow boundary is again prescribed as a bell-shaped function with a maximum value of $\phi^{NP} = 1.0 \times 10^{-6}$. We use a smooth function for the mobility tensor field, i.e., Function 4 shown in Fig. 4(b) and discussed in the previous subsection. The cylindrical magnet has a radius of $R_{mag} = 2.5$ mm and a length of $L_{mag} = 5.0$ mm and is centered below the domain with a distance of 0.2 mm to the bottom wall.

In a first step, we compare three different orientations of the magnet: (a) The magnet is oriented vertically (along the z axis); (b) the magnet is oriented horizontally (along the x axis); (c) the magnet is rotated $45°$ around the y axis.

Figure 5 shows the concentration of the nanoparticles for the three different magnet orientations. For the vertical orientation, the nanoparticles are attracted to the magnet and accumulate at the bottom wall in a circular shape directly above the magnet, similar to experimental results, e.g., presented by Ref. [5]. For the horizontal orientation, the nanoparticles accumulate above the two ends of the magnet, forming two ellipses. For the $45°$ orientation, the nanopar-

ticles form one ellipse above where the edge of the magnet is closest to the bottom wall. Examples in the literature are restricted to a single orientation of a cylindrical magnet of infinite length, e.g., Refs. [2,16]. In contrast, we show that the nanoparticles accumulate above the ends of the magnet—which can obviously not be investigated with a magnet of infinite length.

Further, we here leverage what Derby and Olbert [39] and Caciagli *et al.* [40] stated: Their derived analytical expressions for the magnetic field of magnetized cylinders are especially convenient for applications where magnetic forces on magnetic dipoles are required—nanoparticles being one such example. Our results for the magnetic force are restricted to a cylindrical magnet of finite length with longitudinal magnetization. Similar analytical solutions for cylindrical magnets with arbitrary magnetization can also be derived based on the respective analytical expressions for the magnetic field presented by Caciagli *et al.* [40]. However, if the magnet is of an arbitrary shape, then the magnetic field and force must be evaluated based on numerically solving Maxwell's equations.

Several studies in the literature, e.g., Refs. [2,16–20] reduced the setup to a two-dimensional problem in the XZ plane and assumed the cylindrical magnet to be infinitely long. In this case, the magnetic force can also be expressed analytically, as derived in Ref. [16], and given by

$$F_x = -\mu_0 V^{NP} f(|\boldsymbol{H}|) M_s^2 R_{mag}^4 \frac{x}{2(x^2 + z^2)^3} \tag{26a}$$

and

$$F_z = -\mu_0 V^{NP} f(|\boldsymbol{H}|) M_s^2 R_{mag}^4 \frac{z}{2(x^2 + z^2)^3}, \tag{26b}$$

where the coordinate system is at the center of the magnet and the longitudinal axis of the magnet is perpendicular to the XZ plane. We now compare results based on this assumption of an infinitely long magnet to the results for a finite-length magnet, as derived in this contribution. In both cases, we assume that the magnet has a radius of $R_{mag} = 2.5$ mm and a distance of $\Delta = 0.2$ mm to the bottom boundary of the domain. The cylindrical magnet of finite length has a length of $L_{mag} = 5.0$ mm, as used in the previous examples. For simplicity, we here assume that $f(|\boldsymbol{H}|) = 1.0 = $ const in both cases.
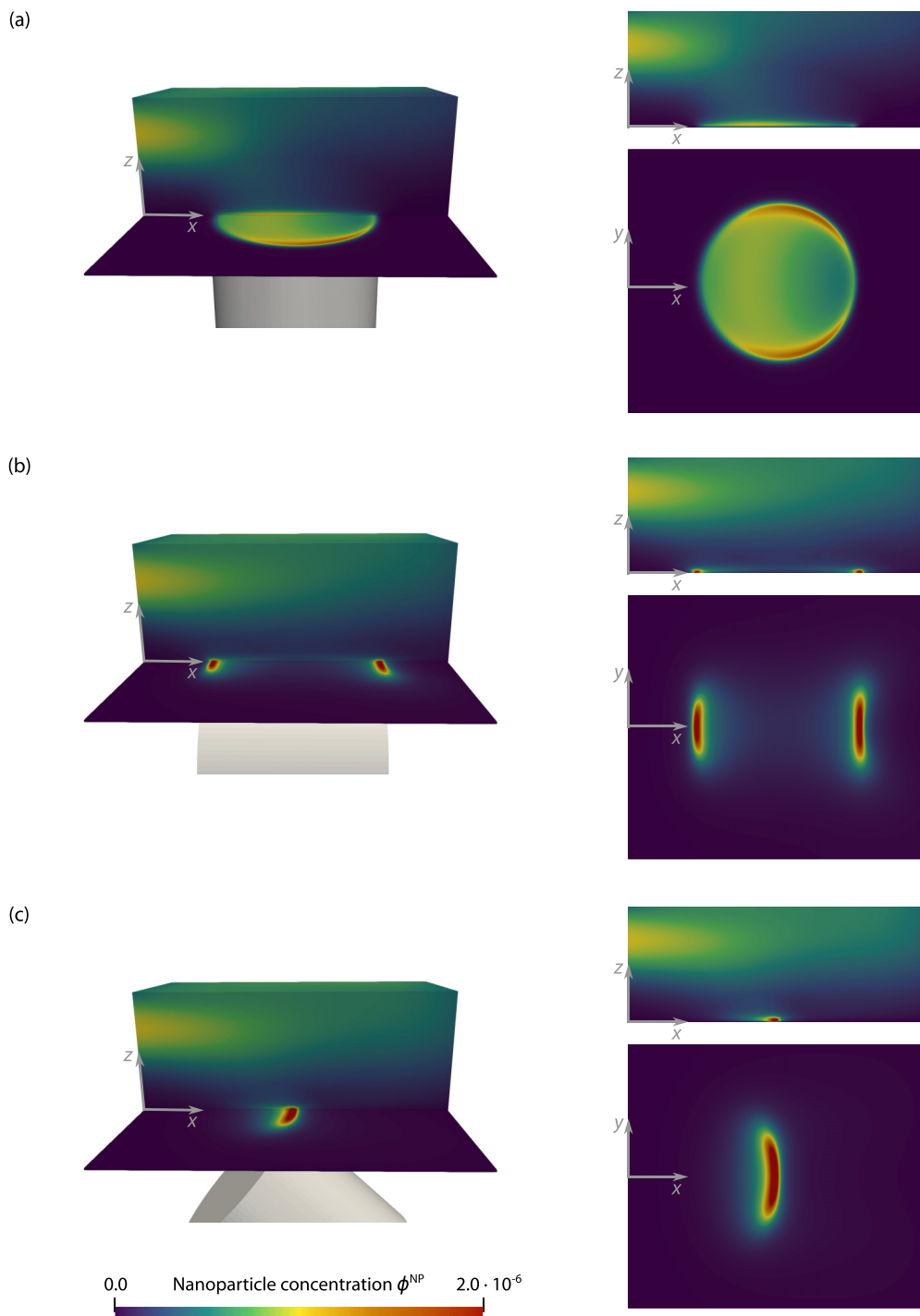
FIG. 5. Results for the nanoparticle capture at $t = 150$ s with a cylindrical magnet of finite length positioned below the domain. (a) The magnet is oriented vertically (along the z axis). (b) The magnet is oriented horizontally (along the x axis). (c) The magnet is rotated 45° around the y axis. The colorbar applies to all plots.

Figure 6 shows the magnetic force and the resulting nanoparticle distributions for the magnet of infinite length compared to the finite-length magnet. As was also evident in Fig. 3, the magnetic force of the finite-length magnet varies along the longitudinal axis of the magnet, and so we compare the force in different slices along the longitudinal axis, in this case the y axis (but the z axis in Fig. 3). Figure 6 shows that the direction of the magnetic force is the same in all cases, but the magnitude is significantly different. For the cylindrical magnet of infinite length, the maximum force in the domain is 0.72 pN. For the finite-length magnet, the maximum force varies considerably depending on the position of the slice: the maximum magnitude is 0.06 pN, 0.09 pN, 1.02 pN, and 1.65 pN for the slices at $y = 0.0$ mm, 1.0 mm, 2.3 mm, and 2.5 mm, respectively. Accordingly, the nanoparticle distributions are also markedly different: The
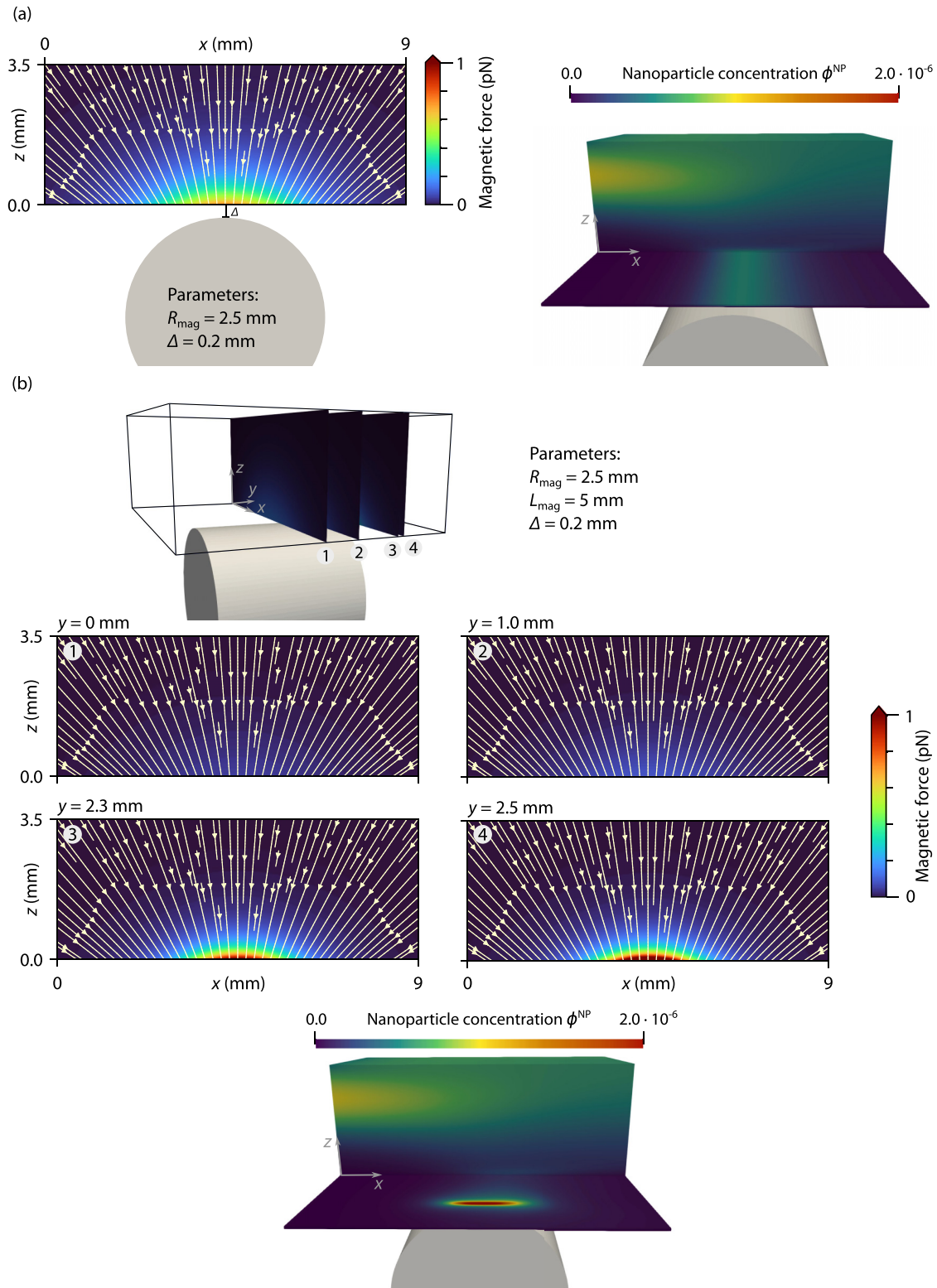
FIG. 6. Comparison of the magnetic force and the resulting nanoparticle distribution for a cylindrical magnet of (a) infinite length and (b) finite length with $L_{\text{mag}} = 5.0$ mm.

nanoparticles accumulate in a higher concentration above the ends of the finite-length magnet than along the infinitely long magnet.

In sum, one has to be aware that the assumption of an infinitely long magnet leads to significantly different results than a finite-length magnet. The analytical solution for the finite-length magnet—as derived in this contribution—provides a simple and computationally efficient way to investigate the transport of nanoparticles in a more realistic setup.
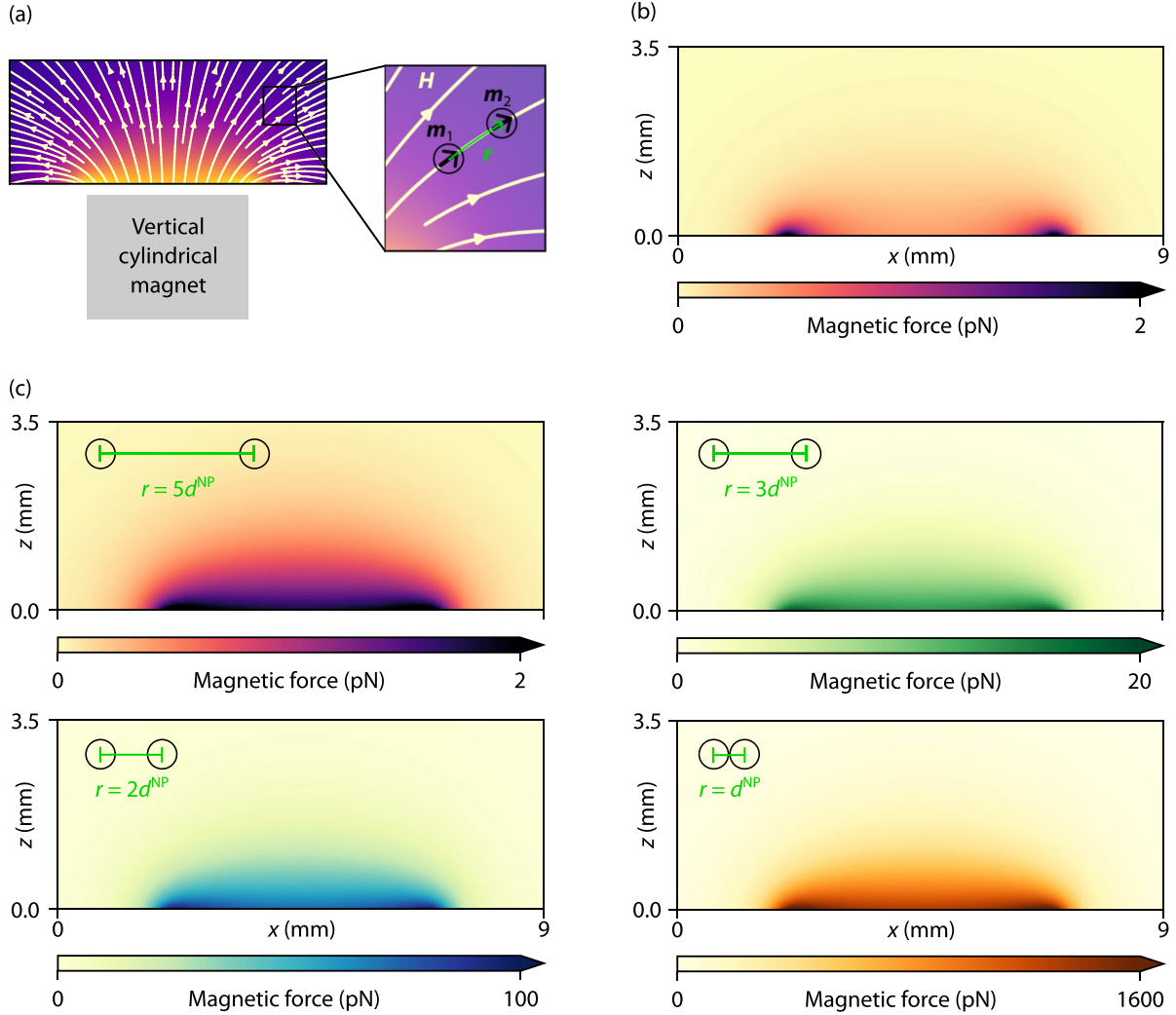
FIG. 7. Comparison of the force exerted by the permanent magnet to the interparticle forces (a) Setup of the investigated case. (b) Externally applied force $\boldsymbol{F}_{\mathrm{mag}}$. (c) Interparticle force $\boldsymbol{F}_{12}$ between two nanoparticles with a distance r between their centers. Note the different orders of magnitude of the forces, which are represented by the different colormaps used in the subfigures.

C. Comparison of the force exerted by the permanent magnet to the interparticle forces

In this contribution, we only consider the external magnetic force the permanent magnet exerts on the nanoparticles. However, the nanoparticles also exert forces on each other, and thus the question arises when these interparticle forces are negligible compared to the force exerted by the permanent magnet. So far in this contribution, we have assumed that the low concentration of nanoparticles ensures that the interparticle distance is large enough for the interparticle forces to be negligible, similar to Refs. [15,16,33–35].

The cutoff length of dipole-dipole interactions in nanoparticle assemblies is about three particle diameters [48]. Assuming that the nanoparticles are more than three particle diameters apart seems reasonable for the nanoparticles dissolved in the flowing fluid in our previous examples. However, when the nanoparticles accumulate at the bottom of the domain, they come very close to each other, and thus interparticle forces might become relevant there. Therefore,

we compare the external magnetic force to the interparticle forces. We use our analytical expressions for the magnetic field and the external magnetic force and build on the force comparison presented by Pálovics and Rencz [11], who investigated a similar setup.

We analyze a simplified example shown in Fig. 7(a): we consider two nanoparticles ① and ② with a diameter of $d^{\mathrm{NP}} = 200\,\mathrm{nm}$ and a distance r between their centers located at $\boldsymbol{x}_1$ and $\boldsymbol{x}_2$. The cylindrical magnet is positioned vertically below the domain [see previous example in Fig. 5(a)]. We assume that the two nanoparticles are aligned with the magnetic field $\boldsymbol{H}$ such that $\boldsymbol{r}$ is parallel to $\boldsymbol{H}$. We again assume $f(|\boldsymbol{H}|) = 1.0 = \mathrm{const}$ for simplicity.

In the following, the nonbold symbols denote the magnitudes of the vectors, e.g., $r = |\boldsymbol{r}|$, and a hat denotes the unit vector in the given direction, e.g., $\hat{\boldsymbol{r}} = \boldsymbol{r}/r$.

As discussed in Sec. II B, the nanoparticles are modeled as point dipoles, with the magnetic moment $\boldsymbol{m}_1$ of nanoparticle ① given by

$$\boldsymbol{m}_1 = V^{\mathrm{NP}}\boldsymbol{H}. \tag{27}$$

The magnetic moment of the nanoparticle is aligned with the applied magnetic field. Since the nanoparticles are much smaller than the computational domain, we assume that $H(x_1) = H(x_2)$ and hence $m_1 = m_2$. The magnetized nanoparticle ① generates a magnetic field H_1 at the position r of nanoparticle ② given by Ref. [38] as

$$H_1 = \frac{1}{4\pi r^3}[3(m_1\hat{r})\hat{r} - m_1]. \tag{28}$$

In our case, $m_1 \parallel r$ and Eq. (28) simplifies to

$$H_1 = \frac{1}{2\pi r^3}m_1. \tag{29}$$

Hence, the total magnetic field H_2^* at the position r of nanoparticle ② is given by

$$H_2^* = H + H_1 \tag{30}$$

and accordingly, the magnetic moment of nanoparticle ② also changes to

$$m_2^* = V^{\mathrm{NP}}H_2^*. \tag{31}$$

Thus, the magnetic moments of both particles increase due to the cross-effects. We could substitute the new values for the magnetic moments back into the previous equations to calculate a second correction of the magnetic field and magnetic moments. In practice, this is not necessary, and we omit it [11,34].

The force F_{12} between the two particles, i.e., the interparticle force, is given by Ref. [49] as

$$\begin{aligned}F_{12} &= \frac{3\mu_0 m_1^* m_2^*}{4\pi r^4}[\hat{r}(\hat{m}_1^*\hat{m}_2^*) + \hat{m}_1^*(\hat{r}\hat{m}_2^*) \\ &\quad + \hat{m}_2^*(\hat{r}\hat{m}_1^*) - 5\hat{r}(\hat{r}\hat{m}_1^*)(\hat{r}\hat{m}_2^*)] \\ &= -\frac{3\mu_0 m_1^* m_2^*}{2\pi r^4}\hat{r}. \end{aligned} \tag{32}$$

We evaluate the interparticle force F_{12} for different distances r between the two nanoparticles: $r \in \{5d^{\mathrm{NP}}, 3d^{\mathrm{NP}}, 2d^{\mathrm{NP}}, d^{\mathrm{NP}}\}$. Figure 7(b) shows the force F_{mag} exerted by the external magnet and Fig. 7(c) the interparticle force F_{12}. For a distance of five particle diameters, the forces are on the same order of magnitude, namely pN. However, the interparticle force strongly increases for smaller distances: for a distance of one particle diameter, it is about three orders of magnitude larger than the force of the external magnet, especially for the particles at the bottom of the domain. This is in good agreement with the results of Pálovics and Rencz [11]. The nanoparticles captured at the bottom of the domain may

thus interact with each other, making interparticle forces relevant. Therefore, if one is interested in the behavior of these captured nanoparticles and the precise profile at the bottom of the domain, then it is necessary to consider the interparticle forces. In this case, the continuum approach used in this study might not be the best choice. Instead, a particle-based approach, which calculates forces on each individual particle, would be more appropriate. However, the focus of our study is not on the fate of individual particles captured at the impenetrable wall or the exact concentration profile at the boundary.

These results underline that one cannot simply assume that the interparticle forces are negligible but must carefully assess whether they are relevant in the configuration studied with the assumptions made.

IV. CONCLUSION

In this contribution, we presented a continuum approach based on the Smoluchowski advection-diffusion equation to model the capture of magnetic nanoparticles under the combined effect of fluid flow and magnetic forces. We included a simple and numerically stable way to consider an impenetrable boundary where the nanoparticles are captured. Further, the analytical expression for the magnetic force of a cylindrical magnet of finite length on the magnetic nanoparticles, which we derived, provides an efficient way to model the capture of magnetic nanoparticles in a more realistic setup in three dimensions.

Since many nanoparticle designs fail in clinical trials, our modeling efforts can help to gain insight into the behavior of magnetic nanoparticles and help to design prototypes. While our expression for the magnetic force is restricted to cylindrical magnets, this is the configuration that is commonly used in experiments, e.g., when studying magnetic nanoparticles in fluidic devices [3–5]. Hence, such an *in silco* model can help with experimental design to limit the number of experiments and thus the costs to the most promising configurations. Finally, the presented model can serve as a precursor to more complex models, e.g., including magnets of arbitrary shape or considering complex biomechanical models coupling the transport of the nanoparticles in the blood vessels with the crossing of the vessel walls and the accumulation in the tumour tissue—both *in vivo* and *in silico* [6,50,51].

[1] N. R. Stillman, M. Kovacevic, I. Balaz, and S. Hauert, In silico modeling of cancer nanomedicine, across scales and transport barriers, npj Comput. Mater. **6**, 92 (2020).

[2] R. L. Hewlin and J. M. Tindall, Computational assessment of magnetic nanoparticle targeting efficiency in a simplified circle of Willis arterial model, Int. J. Mol. Sci. **24**, 2545 (2023).

[3] K. Nguyen, B. Nuß, M. Mühlberger, H. Unterweger, R. Friedrich, C. Alexiou, and C. Janko, Superparamagnetic iron oxide nanoparticles carrying chemotherapeutics improve drug

efficacy in monolayer and spheroid cell culture by enabling active accumulation, Nanomaterials **10**, 1577 (2020).

[4] J. Behr, L. R. Carnell, R. Stein, F. Pfister, B. Friedrich, C. Huber, S. Lyer, J. Band, E. Schreiber, C. Alexiou, and C. Janko, *Invitro* setup for determination of nanoparticle-mediated magnetic cell and drug accumulation in tumor spheroids under flow conditions, Cancers **14**, 5978 (2022).

[5] M. Kappes, B. Friedrich, F. Pfister, C. Huber, R. P. Friedrich, R. Stein, C. Braun, J. Band, E. Schreiber, C. Alexiou, and

C. Janko, Superparamagnetic iron oxide nanoparticles for targeted cell seeding: Magnetic patterning and magnetic 3D cell culture, Adv. Funct. Mater. **32**, 2203672 (2022).

[6] B. Wirthl, C. Janko, S. Lyer, B. A. Schrefler, C. Alexiou, and W. A. Wall, An *in silico* model of the capturing of magnetic nanoparticles in tumour spheroids in the presence of flow, Biomed. Microdev. **26**, 1 (2024).

[7] B. Hallmark, N. J. Darton, and D. Pearce, Modeling the in-flow capture of magnetic nanoparticles, in *Magnetic Nanoparticles in Biosensing and Medicine*, edited by A. Ionescu, J. Llandro, and N. J. Darton (Cambridge University Press, Cambridge, UK, 2019), pp. 151–171.

[8] P. J. Cregg, K. Murphy, and A. Mardinoglu, Inclusion of magnetic dipole–dipole and hydrodynamic interactions in implant-assisted magnetic drug targeting, J. Magn. Magn. Mater. **321**, 3893 (2009).

[9] P. J. Cregg, K. Murphy, A. Mardinoglu, and A. Prina-Mello, Many particle magnetic dipole–dipole and hydrodynamic interactions in magnetizable stent assisted magnetic drug targeting, J. Magn. Magn. Mater. **322**, 2087 (2010).

[10] P. Pálovics, M. Németh, and M. Rencz, Investigation and modeling of the magnetic nanoparticle aggregation with a two-phase CFD model, Energies **13**, 4871 (2020).

[11] P. Pálovics and M. Rencz, Investigation of the motion of magnetic nanoparticles in microfluidics with a micro domain model, Microsyst. Technol. **28**, 1545 (2022).

[12] X. L. Li, K. L. Yao, H. R. Liu, and Z. L. Liu, The investigation of capture behaviors of different shape magnetic sources in the high-gradient magnetic field, J. Magn. Magn. Mater. **311**, 481 (2007).

[13] X. L. Li, K. L. Yao, and Z. L. Liu, CFD study on the magnetic fluid delivering in the vessel in high-gradient magnetic field, J. Magn. Magn. Mater. **320**, 1753 (2008).

[14] A. Munir, J. Wang, and H. S. Zhou, Dynamics of capturing process of multiple magnetic nanoparticles in a flow through microfluidic bioseparation system, IET Nanobiotechnology **3**, 55 (2009).

[15] S. A. Khashan, E. Elnajjar, and Y. Haik, CFD simulation of the magnetophoretic separation in a microchannel, J. Magn. Magn. Mater. **323**, 2960 (2011).

[16] E. P. Furlani and K. C. Ng, Analytical model of magnetic nanoparticle transport and capture in the microvasculature, Phys. Rev. E **73**, 061919 (2006).

[17] E. J. Furlani and E. P. Furlani, A model for predicting magnetic targeting of multifunctional particles in the microvasculature, J. Magn. Magn. Mater. **312**, 187 (2007).

[18] L. Etgar, A. Nakhmani, A. Tannenbaum, E. Lifshitz, and R. Tannenbaum, Trajectory control of PbSe–γ-Fe2O3 nanoplatforms under viscous flow and an external magnetic field, Nanotechnology **21**, 175702 (2010).

[19] S. Shaw, Mathematical model on magnetic drug targeting in microvessel, in *Magnetism and Magnetic Materials* (IntechOpen, 2018).

[20] E. F. Yeo, H. Markides, A. T. Schade, A. J. Studd, J. M. Oliver, S. L. Waters, and A. J. El Haj, Experimental and mathematical modeling of magnetically labeled mesenchymal stromal cell delivery, J. R. Soc. Interface. **18**, 20200558 (2021).

[21] M. Takayasu, R. Gerber, and F. Friedlaender, Magnetic separation of submicron particles, IEEE Trans. Magn. **19**, 2112 (1983).

[22] M. Smoluchowski, Über Brownsche Molekularbewegung unter Einwirkung äußerer Kräfte und deren Zusammenhang mit der verallgemeinerten Diffusionsgleichung, Ann. Phys. **353**, 1103 (1915).

[23] D. Pimponi, M. Chinappi, P. Gualtieri, and C. M. Casciola, Mobility tensor of a sphere moving on a superhydrophobic wall: Application to particle separation, Microfluid. Nanofluid. **16**, 571 (2014).

[24] K. Chen, J. Han, X. Pan, and D. J. Srolovitz, The grain boundary mobility tensor, Proc. Natl. Acad. Sci. USA **117**, 4533 (2020).

[25] P. Wriggers, *Nonlinear Finite Element Methods* (Springer, Berlin, 2008).

[26] O. C. Zienkiewicz, R. L. Taylor, and J. Z. Zhu, *The Finite Element Method: Its Basis and Fundamentals*, 7th ed. (Butterworth-Heinemann, Oxford, UK, 2013).

[27] 4C, Comprehensive Computational Community Code, www.4c-multiphysics.org (2024), accessed: 15.05.2024.

[28] A. N. Brooks and T. J. R. Hughes, Streamline upwind/Petrov-Galerkin formulations for convection dominated flows with particular emphasis on the incompressible Navier-Stokes equations, Comput. Methods Appl. Mech. Eng. **32**, 199 (1982).

[29] V. John and P. Knobloch, On discontinuity—capturing methods for convection—diffusion equations, in *Numerical Mathematics and Advanced Applications*, edited by A. B. de Castro, D. Gómez, P. Quintela, and P. Salgado (Springer, Berlin, 2006), pp. 336–344.

[30] R. Codina, Stabilized finite element approximation of transient incompressible flows using orthogonal subscales, Comput. Methods Appl. Mech. Eng. **191**, 4295 (2002).

[31] T. B. Jones, Fundamentals, in *Electromechanics of Particles* (Cambridge University Press, Cambridge, UK, 1995), pp. 5–33.

[32] E. Tiesinga, P. J. Mohr, D. B. Newell, and B. N. Taylor, CODATA recommended values of the fundamental physical constants: 2018, Rev. Mod. Phys. **93**, 025010 (2021).

[33] E. E. Keaveny and M. R. Maxey, Modeling the magnetic interactions between paramagnetic beads in magnetorheological fluids, J. Comput. Phys. **227**, 9554 (2008).

[34] K. Han, Y. T. Feng, and D. R. J. Owen, Three-dimensional modeling and simulation of magnetorheological fluids, Int. J. Numer. Methods Eng. **84**, 1273 (2010).

[35] M. Woińska, J. Szczytko, A. Majhofer, J. Gosk, K. Dziatkowski, and A. Twardowski, Magnetic interactions in an ensemble of cubic nanoparticles: A Monte Carlo study, Phys. Rev. B **88**, 144421 (2013).

[36] C. Sun, J. S. H. Lee, and M. Zhang, Magnetic nanoparticles in MR imaging and drug delivery, Adv. Drug Delivery Rev. **60**, 1252 (2008).

[37] K. McNamara and S. A. M. Tofail, Nanoparticles in biomedical applications, Adv. Phys.: X **2**, 54 (2017).

[38] J. D. Jackson, *Classical Electrodynamics: International Adaptation*, 3rd ed. (Wiley, Hoboken, NJ, 2021).

[39] N. Derby and S. Olbert, Cylindrical magnets and ideal solenoids, Am. J. Phys. **78**, 229 (2010).

[40] A. Caciagli, R. J. Baars, A. P. Philipse, and B. W. M. Kuipers, Exact expression for the magnetic field of a finite cylinder with arbitrary uniform magnetization, J. Magn. Magn. Mater. **456**, 423 (2018).

[41] B. C. Carlson, Computing elliptic integrals by duplication, Numer. Math. **33**, 1 (1979).

[42] B. C. Carlson and E. M. Notis, Algorithms for incomplete elliptic integrals, ACM Trans. Math. Software **7**, 398 (1981).

[43] W. H. Press, S. A. Teukolsky, W. T. Vetterling, and B. P. Flannery, *Numerical Recipes: The Art of Scientific Computing*, 3rd ed. (Cambridge University Press, Cambridge, UK, 2007).

[44] Wolfram Research, Inc., Mathematica, Version 13.3 (Champaign, IL, 2023).

[45] P. Virtanen, R. Gommers, T. E. Oliphant, M. Haberland, T. Reddy, D. Cournapeau, E. Burovski, P. Peterson, W. Weckesser, J. Bright, S. J. van der Walt, M. Brett, J. Wilson, K. J. Millman, N. Mayorov, A. R. J. Nelson, E. Jones, R. Kern, E. Larson, C. J. Carey *et al.*, SciPy 1.0: Fundamental algorithms for scientific computing in Python, Nature Methods **17**, 261 (2020).

[46] B. Wirthl, Implementation of the analytical expressions for the magnetic field and force of finite-length cylindrical permanent magnet, www.github.com/bwirthl/cylindrical-magnet-functions (2023).

[47] L. M. Roa-Barrantes and D. J. Rodriguez Patarroyo, Magnetic field effect on the magnetic nanoparticles trajectories in pulsating blood flow: A computational model, BioNanoScience **12**, 571 (2022).

[48] G. Barrera, P. Allia, and P. Tiberto, Dipolar interactions among magnetite nanoparticles for magnetic hyperthermia: A rate-equation approach, Nanoscale **13**, 4103 (2021).

[49] D. J. Griffiths, *Introduction to Electrodynamics*, 4th ed. (Cambridge University Press, Cambridge, UK, 2017).

[50] J. Kremheller, A.-T. Vuong, B. A. Schrefler, and W. A. Wall, An approach for vascular tumor growth based on a hybrid embedded/homogenized treatment of the vasculature within a multiphase porous medium model, Int. J. Numer. Methods Biomed. Eng. **35**, e3253 (2019).

[51] B. Wirthl, J. Kremheller, B. A. Schrefler, and W. A. Wall, Extension of a multiphase tumour growth model to study nanoparticle delivery to solid tumours, PLoS One **15**, e0228443 (2020).